Proceedings Paper:
Hooper, F.S., Yuan, R., Revin, D.G. et al. (2023) Optical design and simulation of a cervical scanning probe for polarization-sensitive optical coherence tomography using Ansys Zemax OpticStudio. In: Wojtkowski, M., Yasuno, Y. and Vakoc, B.J., (eds.) Optical Coherence Imaging Techniques and Imaging in Scattering Media V. European Conferences on Biomedical Optics, 2023, 25-30 Jun 2023, Munich, Germany. SPIE, p. 64. ISSN: 0277-786X. EISSN: 1996-756X.

https://doi.org/10.1117/12.2670355

Optical design and simulation of a cervical scanning probe for polarization-sensitive optical coherence tomography using Ansys Zemax OpticStudio

Frances S.W. Hooper *[a], Rui Yuan [a], Dmitry G. Revin [a], Dilly O.C. Anumba [b], Stephen J. Matcher [a]

[a] Department of Electronic and Electrical Engineering, Sir Frederick Mappin Building, University of Sheffield, Sheffield, S1 3JD, UK, [b] Academic Unit of Reproductive and Developmental Medicine, University of Sheffield, Sheffield, S10 2SF UK

ABSTRACT

The leading global cause of death in children under the age of five is due to complications arising from preterm birth (PTB). Although it is not fully understood why PTB can happen spontaneously, it is known that the cervix's collagen rich extracellular matrix remodels prior to both term and preterm labor. *In vitro* polarization-sensitive optical coherence tomography (PS-OCT) has successfully imaged the distribution and 3D alignment of collagen in the cervix, as well as determined birefringence and measured cervical tissue depolarization in healthy tissue samples. The present investigation aims to expand on this research, by implementing *in silico* design, optimization, and simulation techniques for a PS-OCT probe to be used for human *in vivo* cervical scanning. The design considers patient comfort and clinical access as key parameters; ensuring the components are suitable for a colposcope-like probe and commercially available for quick and cost-effective manufacturing. To achieve these aims, the design benefits from using as few components as possible and limiting optical surface reflections.

In this paper we demonstrate that with the use of a cemented gradient index (GRIN) relay system, a field of view (FOV) of up to 6 mm can be achieved, with a back-coupling efficiency of over 73%, on-axis and at up to a 2° scanning angle. Although Huygens point spread function (PSF) lateral resolution reached 81 μm, this paper demonstrates that manual adjustment and optimization of the components can increase this resolution to 12 μm, although at the expense of FOV width reduction. The simulated probe design was verified in preliminary experiments using an in-house built fiber-based OCT engine where high-quality OCT images with wide FOV were obtained from various samples, including healthy human skin.

Keywords: Zemax, Polarization-sensitive optical coherence tomography, colposcopy, spontaneous preterm birth, gradient index lens, vaginal probe

1. INTRODUCTION

Spontaneous preterm birth (sPTB) occurs when a baby is born prior to 37 complete weeks of gestation due to non-medically induced preterm labor and cervical dilation or preterm premature rupture of membranes (PPROM) [1]. In the UK in 2019, 56,458 (8.1%) babies were born preterm. Despite significant developments in perinatal care increasing survival rates, PTB related mortality rates are still extremely high. In the UK in 2019, 74.5% of stillbirths and 72.9% of neonatal deaths (defined as death before 28 complete days after birth) occurred in infants born prematurely [2]. In the same year, an estimated 0.94 million children under the age of 5 died from PTB complications at a global scale, making it the leading cause of death within this age group [3].

While there are known risk factors for sPTB, there is no clear understanding as to why it occurs, making prediction and early prevention difficult [4]. What is known, however, is that the cervix must undergo a structural change prior to labor, known as cervical remodeling [5]. As term labor cannot occur without the remodeling of the cervix, it is concluded that premature cervical remodeling occurs prior to sPTB. This theory was investigated by the recent study of cervical electrical

Optical Coherence Imaging Techniques and Imaging in Scattering Media V, edited by Benjamin J. Vakoc, Maciej Wojtkowski, Yoshiaki Yasuno, Proc. of SPIE Vol. 12632, 126321U
 · 0277-786X · doi: 10.1117/12.2670355

impedance spectroscopy (EIS) at predicting sPTB. EIS can detect abnormalities in cell volume, the conductivity of intracellular and extracellular fluid, and the capacitance of cell plasma membranes leading to lower cervical impedance which correlates with resulting preterm labor. However, the relation of these changes to cervical remodeling is still unclear [6]. The implementation of imaging modalities that can study cervical collagen during remodeling should therefore help to identify triggers for sPTB and provide preventative treatments to help patients carry to term.

Optical coherence tomography (OCT) is one such imaging technique which has been found to successfully image and quantify collagen fiber orientation in cervical samples [7-9]. Due to its high resolution [10], fast imaging speed in 3D and deep tissue penetration of up to 2 mm [11], OCT can show distinguishable differences in collagen composition in different cross-sectional regions of the cervix [7-9, 12, 13]. Despite this success, conventional OCT techniques struggle to accurately assess collagen structure [7, 8]. Instead, the implementation of polarization imaging can be used to evaluate anisotropic structures, such as the highly organized collagen fibers in the cervix [14]. Polarization-sensitive OCT (PS-OCT) is a functional extension of OCT which can identify depth-resolved phase retardance and birefringence by measuring the polarization state of backscattered light from the cervical collagen, allowing it to be differentiated from its surrounding tissues [15]. PS-OCT has shown success in its ability to image the distribution and 3D alignment of collagen in the cervix, as well as determine birefringence, measure cervical tissue depolarization, and differentiate high collagen tissue from other tissue structures such as the cervical epithelium [16]. It has potential to monitor the changes in cervical microstructure during remodeling in pregnancy, and ultimately during premature cervical remodeling. The recent progress in this research, however, is mainly limited to *in vitro* data studies. For this modality to have a clinical diagnostic application, it must be delivered to the cervix with appropriate optics for *in vivo* studies.

In this paper we have designed and simulated an *in vivo* probe using Ansys Zemax optical software, OpticStudio. By implementing the *in silico* design and optimization features offered by OpticStudio, we were able to design a suitable optical probe to constitute the sample arm of an eventual single mode fiber (SMF) based PS-OCT system [17], which would allow the light to propagate in both direction, through the vagina to the cervix and back. Key requirements for the optical components of this design were: (i) to function with a 1300 nm center wavelength swept source laser; (ii) to be small enough to ensure the probe has a diameter for comfortable insertion into the vagina; and (iii) to provide adequate probe length to reach the cervix from outside the patient. Additionally, the optical components should be commercially available off-the-shelf to reduce costs and construction time and should aim for optimal transmission and image quality.

2. SELECTION OF PROBE OPTICAL COMPONENTS

2.1 Probe optics parameters

To abide by the key requirements listed above, several parameters were established for the probe design to ensure its clinical usability. Size based parameters for the probe were established from the measurements of a cervical EIS probe previously designed for a similar study [6]; the insertable probe end was to be at least 140 mm in length, and the diameter of the optics were not to exceed 7.5 mm. To ensure the optical components were compatible with in-house OCT systems for bench testing and future SMF-based PS-OCT systems for clinical studies, the components had to be suitable for use at 1300 nm wavelengths and be compatible with SMF fibers.

To simulate the laser light propagation from the SMF fiber to the probe optics, Gaussian beam theory was applied. Single-mode fibers should be modeled using their mode field diameter (MFD) and the light source's wavelength, rather than the numerical aperture (NA) of the fiber (0.14 [18]), as Gaussian beams act like collimated bundles of rays within their Rayleigh range (z_R) and diverge at an approximate linear rate in the far field ($z >> z_R$) [19]. To implement this theory in OpticStudio, the Rayleigh range of the SMF was calculated to be 51 μm according to Eq. 1[19]:

$$z_R = \frac{\pi}{\lambda} \cdot \left(\frac{MFD}{2}\right)^2 \quad (1)$$

where the *MFD* of the SMF is 9.2 μm for a 1310 nm wavelength (λ) [18]. The beam radius (w) at a far field distance (z) of 1.0 mm was then calculated to be 91 μm according to Eq. 2[19]:

$$w(z) = \frac{MFD}{2} \cdot \sqrt{1 + \left(\frac{z}{z_R}\right)^2} \quad (2)$$

These values are shown in Table 1, where the 1.0 mm far field distance (z) is the "thickness" of Surface 1, and the 91 μm beam radius ($w(z)$) is the "semi-diameter" of the STOP surface. To model the Gaussian beam, the System Aperture Type was set to *Float by Stop Size*, the System Apodization Type was set to *Gaussian*, and the Apodization Factor was set to *1*.

Table 1. OpticStudio Lens Data Editor information for Gaussian beam projection from a single mode fiber.

Surface	Type	Radius/ mm	Thickness/ mm	Semi-Diameter/ mm
OBJECT	Standard	Infinity	0.000	0.000
1	Standard	Infinity	*1.000*	0.000
STOP	Standard	Infinity	*Variable*	*0.091*

2.2 FiberPort Collimator/Coupler and MEMS Scanning Mirror

To collimate the diverging light from the SMF, a commercial collimating/coupling lens with a diameter of 5 mm and focal length of 7.5 mm was selected. The lens is housed within a cage mountable FiberPort that allows for finite adjustment of the lens' tilt and decenter for calibration in the physical probe prototype. In OpticStudio, the "thickness" of the STOP surface from Table 1 was defined as a *variable* value and adjusted with the *Angular Radial* Criterion in the *Quick Adjust* optimization feature, positioning the collimating lens at an appropriate distance to the STOP surface to collimate the beam. The collimated beam from this lens has a diameter of 1.36 mm and is propagated towards a Micro Electronic Mechanical Systems (MEMS) scanning mirror, where the light is reflected at 45° to travel down the insertable end of the probe. The mirror will be integrated within its actuator, which can be driven to tilt the mirror by up to ± 5° about the X and Y axes for scanning.

2.3 Relay System

To channel the light to the cervix, an endoscopic relay system is required. There are three main types of relay system designs available for this purpose: (i) a conventional relay system; (ii) a rod lens system; and (iii) a gradient index (GRIN) lens. The conventional system can be made of multiple repeating relay stages which each consist of multiple lenses to cover the required probe length. One such design of a conventional system by Liang (2011) can yield a high lateral resolution (Huygens PSF, 14 μm) and low field curvature (0.2 mm at a field of view (FOV) of 2.0 mm). Although off-the-shelf lenses could be used, this conventional system design requires 14 custom lenses to reach over the 140 mm length requirement of the probe, creating 56 optical surface reflections as the light passes through the system to the cervix and back again, resulting in power loss [20, 21]. The mounting of 14 lenses within the physical probe prototype at their specific positions would also be difficult to achieve. A rod lens system is an alternative that would reduce the number of lenses required for propagating light over the 140 mm insertable distance. However custom design lenses would be necessary for its use in this project, increasing probe production time and cost.

Instead, a commercially available GRIN lens system was implemented into this probe design. GRIN lenses have a gradient of refractive indexes along their optical axis [22], allowing the light rays to be "bent" within a single rod-like lens (Figure 1). The chosen lens system is a commercially available 157 mm long GRIN lens system with a 2 mm diameter. This system also includes an objective lens at the distal end of the probe, further reducing the optical surface reflections and optical losses. The GRIN lens also provides a lateral resolution (Huygens PSF, 27 μm) and field curvature (0.22 mm at a FOV of 1.7 mm) comparable to the conventional relay system by Liang (2011).

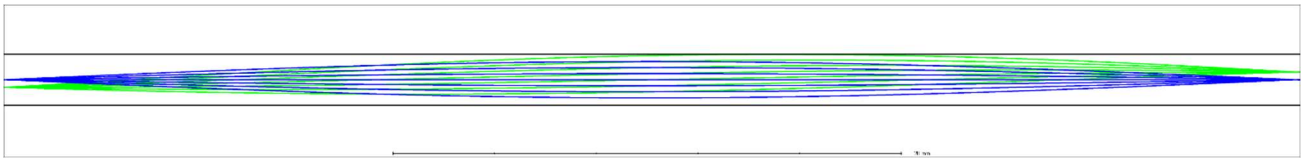

Figure 1. “Bending” propagation of light at different object-space field angles through a 0.5 pitch GRIN lens.

2.4 Focusing lens

A focusing lens was required to couple the reflected collimated beam from the scanning mirror to the GRIN lens for propagation through the insertable probe end. A commercially available 4 mm diameter plano-convex lens was ultimately selected for the design. The chosen lens has a focal length of 8.0 mm and produces a NA of 0.087 when used within the probe design, optimal for coupling light into the GRIN system. The GRIN and focusing lens positions within the design were achieved with the *Spot Size Radial* Criterion in the *Quick Adjust* optimization feature in OpticStudio, by focusing the collimated light onto the first surface of the GRIN lens system.

3. OPTIMIZATION AND ANALYSIS OF THE PROBE COMPONENT POSITIONS

The full 3D layout of the cervical scanning probe design is shown in Figure 2, with the components labeled. Before optimization, the scanning feature of the MEMS mirror was simulated. Using *Coordinate Breaks* and the *Multi-Configuration Editor* in OpticStudio, the mirror was tilted by 1° steps about the X axis, from 0° (on-axis) to + 5° using the PRAM operand. Due to the dimensions of the focusing lens and GRIN system, the system experienced some light loss due to vignetting at high MEMS scanning angles. 35% of light was lost at + 3° angle, and 100% of light was lost at + 4° and higher angles. The maximum scanning angle range of the mirror was therefore set to ± 2° about the X and Y axes, where light transmittance was 98%.

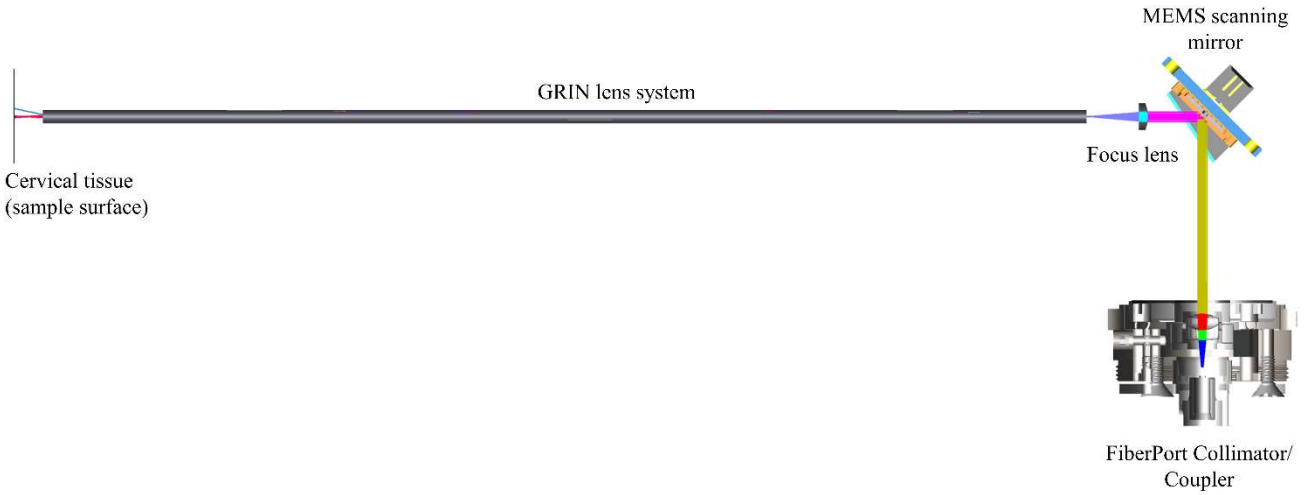

Figure 2. Labelled 3D layout of the cervical scanning probe created in the non-sequential mode of Zemax OpticStudio.

3.1 Optimization and analysis of probe component positions

Using the *Optimization Wizard* in OpticStudio, the optical probe design was optimized for *Spot Size RMS*. The system was optimized for all configurations, relating to the scanning mirror angles of 0°, + 1°, and + 2° about the optical axis. This was to disperse any aberrations across the probe’s field of view (FOV). The layout of the optical probe design is shown in Figure 3 with (a) on-axis and (b) maximum scanning angle light propagation.

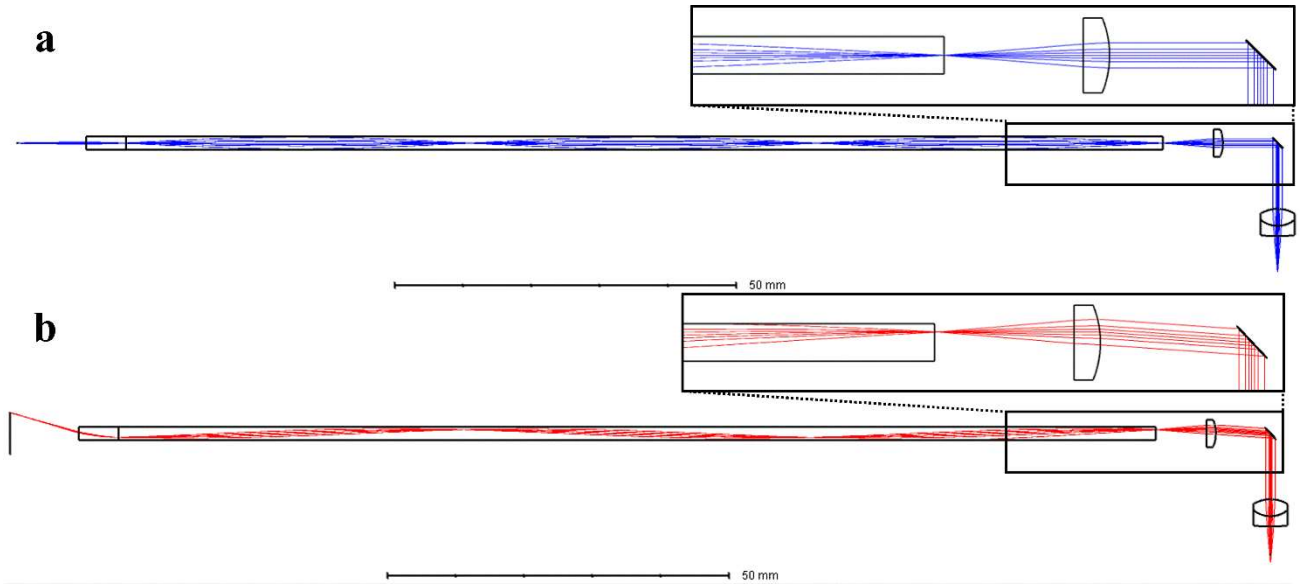

Figure 3. 2D layout of the cervical scanning probe with scanning mirror angles (a) on-axis and (b) +2°.

At the maximum scanning mirror angle of + 2°, the chief ray incident angle was -16.2°, meaning the system is not telecentric in the imaging plane, as shown by the light propagation in Figure 3(b). This is due to the magnification of the GRIN Objective and allows the design to have a wider FOV not limited by the diameter of the optics used. The vertical FOV on the sample surface was 6.0 mm, which was 1-2 mm wider than previously cited for OCT systems used to image the cervix [7, 12, 13]. The lateral resolution of the probe was calculated from the full width half maximum (FWHM) of the cross-sectional Huygens PSF generated in OpticStudio. The on-axis lateral resolution of the probe was 81 µm and lateral resolution at +2° scanning mirror angle was 39 µm. This lateral resolution is considered to be quite poor for a near-infrared OCT system [10], and so further improvements to the probe design were required.

The back-coupling efficiency of the probe was also evaluated, by creating a *Double Pass* of the probe's optics and assigning the sample surface material to a retro-reflective mirror. This was to simulate cervical tissue's reflectivity of OCT light at scanning angles outside of 0°. The system performed well, with high back-coupling efficiency on-axis and at +2° mirror angle, of 75% and 74% respectively. These results are presented under the *Initial design* parameters in Table 2.

3.2 Optimizing for lateral resolution

To improve lateral resolution, the distances between several optical components were set to variables and the probe design was optimized again for *Spot Size RMS* in all configurations. This changed the distance between the focusing lens and both the MEMS mirror and GRIN system, improving lateral resolution results. However, unregulated optimization of the design for *Spot Size RMS* alone negatively affected other key performance metrics, including the light loss due to vignetting and therefore the back-coupling efficiency of the system. To mitigate these effects, manual adjustment of the optical component positions was carried out in conjunction with the *Optimization Wizard*, with the aim of reducing lateral resolution whilst maintaining high light transmittance and back-coupling efficiency. The results of this adjustment are presented in Table 2, under the *Maximum resolution design*. These changes led to the on-axis lateral resolution being improved to 12 µm and lateral resolution at +2° scanning mirror angle improved to 10 µm. However, the resulting probe's FOV was drastically reduced to 1.45 mm, much lower than the 4-5 mm FOV of other OCT systems [7, 12, 13].

Through continued experiments of slightly adjusting the optical component positions in the design, it was found that the FOV could be improved, but at the expense of the lateral resolution. These changes, however, had little effect on the chief ray incident angle and the back-coupling efficiency of the probe design (Table 2). At this research stage, it is unknown whether high FOV or high lateral resolution would be preferred when imaging cervical collagen with the finalized PS-

OCT system in clinical studies. Therefore, the exact parameters for the probe's lateral resolution and FOV will be chosen after it is trialed and assessed on *in vivo* cervical samples.

Table 2. Effect of manual adjustment of lens positions on key performance metrics

Probe design	**Lateral resolution/ µm**		**Chief ray incident angle/ °**	**Vertical FOV/ mm**	**Back-Coupling Efficiency/ %**	
	on-axis	**at + 2°**	**at + 2°**	**at + 2°**	**on-axis**	**at + 2°**
Initial design	81	39	-16.2	6.02	74.67	73.93
Maximum resolution design	12	10	-15.8	1.45	74.67	73.27

3.3 Benchtop assessment of probe layout

The optical components selected for the probe design were obtained from their commercial sources to build the simulated probe on the benchtop. The components were then arranged and aligned respectively to their corresponding positions as in the OpticStudio simulation layout. The benchtop realization of the design was then tested as the sample arm within an in-house built fiber-based non-polarizing OCT system with a 1309 nm FDML laser (the OCT engine). A similar set of optics to the probe were used in the reference arm of the OCT engine. The MEMS mirror within the probe was set to scan at an angle of ± 2.5° about the X axis. Preliminary results were gathered from two samples: an uncoated, transparent, plastic diffraction grating with a semi-spherical profile and a 0.256 mm pitch (Figure 4(a)); and the palm area of human skin. A typical B-scan of the grating containing 600 A-scans is presented in Figure 4(b), showing 19 distinct pitches, therefore resulting in a scanning FOV of ~4.9 mm. It was also found that by adjusting the position of the grating from the distal end of the probe, a scanning FOV of ~6.6 mm could be obtained. A typical B-scan containing 600 A-scans of the palm of the hand is presented in Figure 5, showing distinct laying of the skin surface, stratum corneum and epidermis/ dermis. Although the lateral and axial resolution of the probe was not fully characterized in these preliminary experiments, Figure 5 clearly demonstrates a qualitative capability of the present probe to produce well defined OCT images.

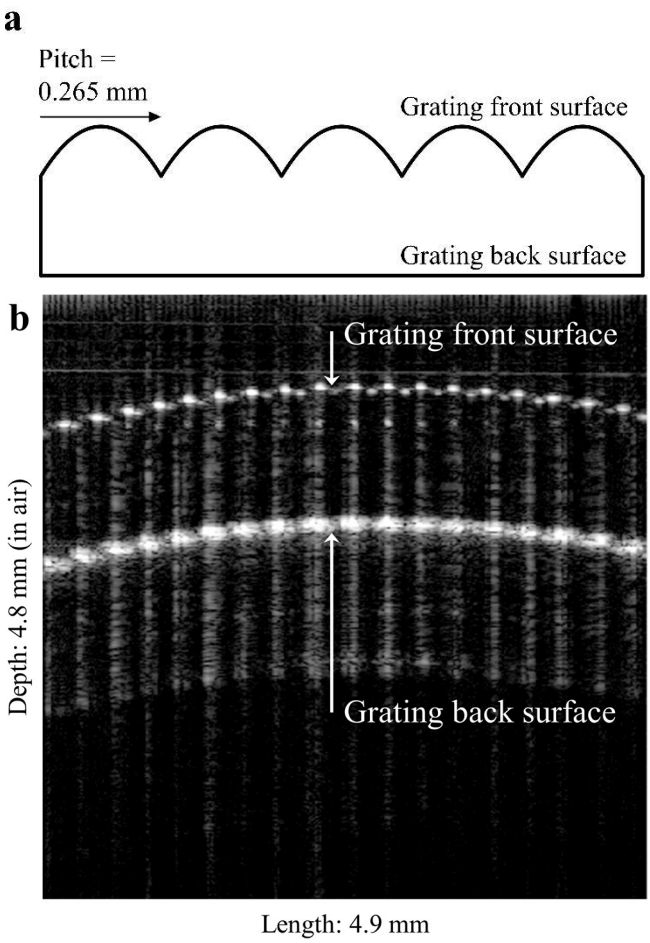

Figure 4. Plastic diffraction grating: (a) labeled semi-spherical profile of grating sample with a 0.256 mm pitch; (b) typical OCT B-scan containing 600 A-scans of the grating taken with in-house built non-polarizing OCT engine.

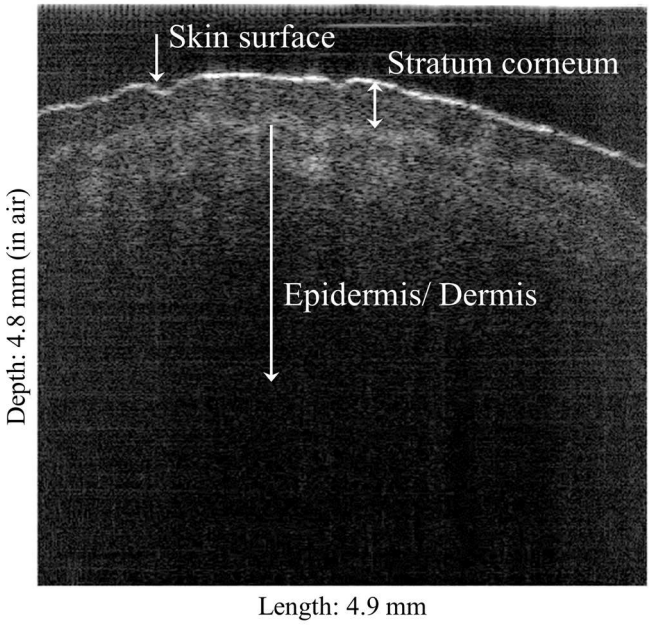

Figure 5. Typical OCT B-scan containing 600 A-scans of the palm region of human skin, taken with in-house built non-polarizing OCT engine.

4. CONCLUSION

In this paper, the design, simulation, and verification of an OCT-compatible cervical scanning probe was demonstrated. The design was carefully considered for the comfort of patients and benefit of clinicians by using long and narrow, commercially available optical components that are cheaper and easier to access than custom alternatives. By creating and optimizing the design *in silico*, this paper shows that a full analysis of the design can be achieved without the need to purchase the optical components. The simulation showed that the optical probe design was non-telecentric and can provide high light transmittance and coupling efficiency, with either high lateral resolution or wide FOV. The *in silico* optimization and simulation of the design has already benefited practical work, providing guidance during probe construction and parameter goals for comparison during bench testing. By preliminary bench testing the simulated design, we have confirmed the probe can function appropriately with a near-infrared OCT engine and provide well defined OCT images with adequate FOV. Further optimizations of the probe design and experimental tests will be conducted. OpticStudio will continue to be used in this research to analyze polarization-based optical effects, further optimize the probe design, and aid in the assessment of further experimental tests conducted on the probe, on benchtop and in a clinical *in vivo* setting.

REFERENCES

[1] M. J. Stout, R. Busam, G. A. Macones *et al.*, "Spontaneous and indicated preterm birth subtypes: interobserver agreement and accuracy of classification," Am J Obstet Gynecol*,* 211(5), 530.e1-4 (2014).

[2] E. S. Draper, I. D. Gallimore, L. K. Smith *et al.*, [MBRRACE-UK Perinatal Mortality Surveillance Report: UK Perinatal Deaths for Births from January to December 2019], (2021).

[3] J. Perin, A. Mulick, D. Yeung *et al.*, "Global, regional, and national causes of under-5 mortality in 2000-19: an updated systematic analysis with implications for the Sustainable Development Goals," The Lancet Child & Adolescent Health*,* 6(2), 106-115 (2022).

[4] J. P. Vogel, S. Chawanpaiboon, A.-B. Moller *et al.*, "The global epidemiology of preterm birth," Best Practice & Research Clinical Obstetrics & Gynaecology*,* 52, 3-12 (2018).

[5] S. M. Yellon, "Contributions to the dynamics of cervix remodeling prior to term and preterm birth," Biology of Reproduction*,* 96(1), 13-23 (2016).

[6] D. O. C. Anumba, V. Stern, J. T. Healey *et al.*, “Value of cervical electrical impedance spectroscopy to predict spontaneous preterm delivery in asymptomatic women: the ECCLIPPx prospective cohort study,” Ultrasound in Obstetrics & Gynecology, 58(2), 293-302 (2021).
[7] Y. Gan, W. Yao, K. M. Myers *et al.*, “Analyzing three-dimensional ultrastructure of human cervical tissue using optical coherence tomography,” Biomedical Optics Express, 6(4), 1090-1108 (2015).
[8] W. Yao, Y. Gan, K. M. Myers *et al.*, “Collagen Fiber Orientation and Dispersion in the Upper Cervix of Non-Pregnant and Pregnant Women,” Plos One, 11(11), (2016).
[9] J. P. McLean, Y. Gan, T. H. Lye *et al.*, “High-speed collagen fiber modeling and orientation quantification for optical coherence tomography imaging,” Optics Express, 27(10), 14457-14471 (2019).
[10] S. Aumann, S. Donner, J. Fischer *et al.*, [Optical Coherence Tomography (OCT): Principle and Technical Realization] Springer International Publishing, (2019).
[11] B. Liu, and M. E. Brezinski, [Optical Coherence Tomography] Elsevier, Oxford, 4.14 (2014).
[12] Y. Gan, W. Yao, K. M. Myers *et al.*, "An automated 3D registration method for optical coherence tomography volumes." 2014, 3873-6 (PMC6080205).
[13] J. Chue-Sang, Y. Bai, S. Stoff *et al.*, “Use of Mueller matrix polarimetry and optical coherence tomography in the characterization of cervical collagen anisotropy,” Journal of Biomedical Optics, 22(8), 1-9 (2017).
[14] S. J. Matcher, “A review of some recent developments in polarization-sensitive optical imaging techniques for the study of articular cartilage,” Journal of Applied Physics, 105(10), 102041 (2009).
[15] B. Baumann, “Polarization Sensitive Optical Coherence Tomography: A Review of Technology and Applications,” Applied Sciences, 7(5), 474 (2017).
[16] W. Li, B. F. Narice, D. O. Anumba *et al.*, “Polarization-sensitive optical coherence tomography with a conical beam scan for the investigation of birefringence and collagen alignment in the human cervix,” Biomedical Optics Express, 10(8), 4190-4206 (2019).
[17] Z. Ding, Q. Tang, C. P. Liang *et al.*, “Imaging Spinal Structures With Polarization-Sensitive Optical Coherence Tomography,” IEEE Photonics Journal, 8(5), 1-8 (2016).
[18] [Single Mode Fiber with Ø900 μm Hytrel Jacket Specification Sheet], (2015).
[19] A. M. K. Kowalevicz, Jr., and F. Bucholtz, [Beam Divergence from an SMF-28 Optical Fiber], Naval Research Laboratory, Washington, DC(2006).
[20] J. Kang, X. Li, M. Wan *et al.*, “Optical design and simulation of an integrated OCT and video rigid laryngoscope,” Journal of Innovative Optical Health Sciences, 13(03), 2040002 (2020).
[21] R. Liang, [Endoscope optics] SPIE, 8 (2011).
[22] M. J. Riedl, [Special Optical Surfaces and Components] SPIE Press, Bellingham, WA(2001).